

# Individual Particle Based Description of Atmospheric Dispersion: a Dynamical Systems Approach

Tímea Haszpra<sup>\*</sup> and Tamás Tél<sup>\*,†</sup>

<sup>\*</sup> MTA–ELTE Theoretical Physics Research Group, Pázmány P. s. 1/A, H-1117 Budapest, Hungary

<sup>†</sup> Department of Theoretical Physics, Eötvös Loránd University, Pázmány P. s. 1/A, H-1117 Budapest, Hungary

**Abstract** We argue that a proper treatment of material dispersion should be based on individual particle tracking using realistic size and density. The effect of turbulent diffusion and the scavenging of particles by precipitation are shown to be treatable as stochastic perturbations of the deterministic Newtonian equation of motion. This approach enables one to investigate the chaotic aspects of particle dispersion by means of dynamical systems concepts. Topological entropy is shown to be in this context the growth rate of material lines, which can be considered to provide a novel characterization of the state of the atmosphere. The deposition process is found to be well characterizable by the escape rate (being a measure of the strength of the exponential decay of the number of particles not yet reached the surface), which might depend on local turbulence and rain intensity. The variability of the dispersion process due to the difference between different meteorological forecasts within an ensemble forecast are also illustrated. Examples are taken from volcanic eruptions and the Fukushima accident.

## 1 Introduction

The concepts of chaos theory apply to any nonlinear system. Nowadays they are also widely used in different treatments of climate dynamics, as some chapters of this book also illustrate. The most appropriate appearance of dynamical systems theory is in conceptual climate models since chaos is basically a low-dimensional phenomenon. Primarily, it is a feature of temporal dependence without any spatial extension. Chaos is thus a property of systems describable by ordinary differential equations. The often heard statement that weather is chaotic should therefore be interpreted

in a symbolic sense: weather, in which spatial features are essential, is more complex than chaotic. It is basically turbulent in accordance with the fact that weather is described by the partial differential equations of hydrodynamics. (In spite of the differences between chaos and turbulence, some features might be in common, like e.g. the fact that both phenomena are unpredictable.) As a consequence, all aspects of climate dynamics related to essential spatial features and requiring thus a description in terms of partial differential equations are more complicated than chaotic.

There is one class of phenomena, relevant both in weather- and climate-related contexts, namely the dispersion of particles, which is a chaotic process. This is so because the traditional description of any flow occurs in the Eulerian picture, and implies the determination of the velocity field. The advection of particles can, however, be treated as a phenomenon sitting on top of the Eulerian description. Particles basically follow the fluid velocity at their instantaneous position, and their motion, a Lagrangian feature, can be considered as one *driven* by the Eulerian flow. Particle trajectories, which are functions of time only, can thus basically be obtained as solutions of ordinary differential equations containing the velocity field (which itself fulfills a partial differential equation) as a known input function. In this sense advection is a clearly chaotic phenomenon as the term “chaotic advection” (Aref, 1984) expresses.

In the last decades the demand for precise tracking and forecasting of atmospheric pollutants has increased due to the growing interest in environmental problems and, consequently, to the requirements for detailed prediction of health and economic hazards. Recent events like volcanic eruptions (e.g. Mount St. Helens (1980), Pinatubo (1991), Eyjafjallajökull (2010)) and pollutant spreading from industrial accidents (e.g. Fukushima (2011)) underline the need for investigating pollutant dispersion in the atmosphere. Aerosol particles from different sources may be advected far away from their initial position and may cause air pollution episodes at distant locations. As discussed above, a Lagrangian description is needed in all cases when one is interested in pollutant trajectories<sup>1</sup>.

A broad class of the currently used particle-tracking models tracks “ghost particles” (computational particles): any of these particles is assumed to be point-like, and carries an artificial mass which decays in time (e.g. HYSPLIT (Draxler and Hess, 2004), FLEXPART (Stohl et al., 2010)). The properties of these particles usually do not coincide with those of any real pollutant particle. In contrary, such particles typically follow the path of

---

<sup>1</sup>For describing pollutant concentrations, also Eulerian methods are available, in terms of advection-diffusion-sedimentation equations, but they are not based on individual particles, and thus cannot reflect chaos-related properties.

an air parcel (ideal passive tracer), gravitational settling does not have an effect on the motion of “ghost particles”. The mass  $m$  (whose numerical value might be on the order of kilograms) attributed to the ghost particle is time-dependent and decreases due to dry and wet deposition according to the equation:

$$\frac{dm(t)}{dt} = -C(\mathbf{r}(t), t)m(t), \quad (1)$$

where  $C(\mathbf{r}(t), t)$  is a location and time-dependent coefficient. It is the quantity  $C$  which is used to describe effects like gravitational settling, and dry or wet deposition.

In addition, in this approach a ghost particle is thought to be the center of mass of a large amount of adjacent pollutants. This assumption only holds if neighboring particles remain together forever. It is well-known, however, that advection is typically chaotic (Aref, 1984) and the nature of chaotic dynamics implies that an initially small, compact ball becomes rapidly deformed and strongly stretched. A measure of this strong deviation of neighboring particles is the so-called Lyapunov exponent (Ott, 1993). In a pictorial representation, the ball of real particles becomes deformed into a complicated, filamentary shape of large extent, see Figure 1. We should therefore conclude that the physical reality of “ghost particle” models is strongly questionable.

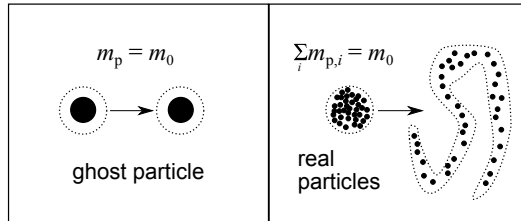


**Figure 1.** Comparison of the dispersion of a “ghost particle” and of real particles after some time, in the atmospheric context, after a few days. The total mass of the real particles of individual mass  $m_{p,i}$  is equal to the mass  $m_p = m_0$  of the ghost particle.

A faithful approach in the Lagrangian picture thus requires *real* particles: the particles in these models have fixed, realistic size and density (Heffter and Stunder, 1993; Searcy et al., 1998). However, the currently available models of this type do not take into account important effects like small-scale turbulence and the scavenging of particles by precipitation.

## 2 The RePLaT Lagrangian Dispersion Model

In order to cope with these effects, we expanded the validity of the available models (Heffter and Stunder, 1993; Searcy et al., 1998) and developed a relatively simple one, the Real Particle Lagrangian Tracking (RePLaT) model which is able to describe real physical processes reasonably well (Haszpra and Tél, 2013a). The model tracks individual aerosol particles with realistic size and density, and takes into account more processes than other “real particle” models. Since RePLaT describes the motion of realistic aerosol particles, it is also suitable for the investigation of the dispersion and deposition processes from a dynamical systems point of view.

The equation of motion for the particle trajectory  $\mathbf{r}_p(t)$  is derived from Newton’s equation. The drag force depends on the particle Reynolds number that quantifies the relation of hydrodynamical and viscous acceleration due to the relative velocity between particle and fluid. Scale analysis reveals that the horizontal velocity of a small aerosol particle takes over the actual local wind speed practically instantaneously, whereas vertically the terminal velocity also has to be taken into account besides the vertical velocity component of air. Therefore a particle is advected by the wind components in the horizontal direction, and its vertical motion is, in addition, influenced by its terminal velocity  $w_{\text{term}}$  which depends on the size  $r$  and density  $\rho_p$  of the particle, as well as, on the density  $\rho$  and viscosity  $\nu$  of the air at the location of the particle:

$$\frac{d\mathbf{r}_p}{dt} = \mathbf{v} + w_{\text{term}}\mathbf{n}, \quad (2)$$

where  $\mathbf{n}$  is the vertical unit vector pointing upwards. For aerosol particles of size of at most  $12\ \mu\text{m}$  and with density about  $\rho_p = 2000\ \text{kg/m}^3$  Stokes’ law is valid during the full motion, and hence the terminal velocity is

$$w_{\text{term}} = -\frac{2}{9} \frac{\rho_p r^2}{\rho \nu} g. \quad (3)$$

Since the meteorological data utilized by the dispersion model have coarse resolution without resolving turbulent diffusion, the effect of small-scale turbulent diffusion on the particles is built into the model as a stochastic process. Within the planetary boundary layer the computation of the vertical turbulent diffusivity is based on the Monin–Obukhov similarity theory (see e.g. Dyer (1974); Troen and Mahrt (1986)), while the horizontal turbulent diffusivity is assumed to be constant in both the boundary layer and in the free atmosphere. The equation of motion completed by the impact of turbulent diffusion is

$$\frac{d\mathbf{r}_p}{dt} = \mathbf{v} + w_{\text{term}}\mathbf{n} + \xi\mathbf{D}, \quad (4)$$

where  $\xi$  is a random walk process and  $\mathbf{D}$  represents the turbulent diffusion coefficient in the different directions, which might be location- and time-dependent.

A further novel feature of the model is the application of the impact of precipitation on individual particles by a random process which depends on precipitation intensity. For the parametrization of wet deposition, we have taken over what is used in the corresponding Eulerian approach (Seinfeld and Pandis, 1998). There the impact of wet deposition is taken into account via Eq. (1) with  $C = k_w$  called the wet deposition coefficient (or scavenging coefficient). This implies that after a short time  $\Delta t$ , locally a fraction  $1 - \exp(-k_w \Delta t) \approx k_w \Delta t$  of mass becomes converted into wet material within the computational cell. We use this relationship to incorporate wet deposition into our model. We consider wet deposition as a random process that results in a particle being captured by a raindrop in time  $\Delta t$  with probability

$$p = 1 - \exp(-k_w \Delta t). \quad (5)$$

Thereby the radius of the particle suddenly increases to the mean radius  $r_{\text{rain}}$  of raindrops which is on the order 100  $\mu\text{m}$  or larger. The trajectory of the “new” particle (a particle that turned into a raindrop) is computed using the terminal velocity based on the new properties of the particle, and follows typically from the quadratic drag law. The “new” particle does not leave the atmosphere instantaneously, but falls through the air according to the equation of motion (4), with the terminal velocity

$$w_{\text{term}} = -\frac{8}{3} \frac{\rho_{\text{rain}} r_{\text{rain}} g}{\rho C_D} \quad (6)$$

of raindrops, where  $C_D = 0.4$  is the drag coefficient for spheres.

There are different parametrizations available for the typical radius of the raindrops (Sportisse, 2007). In RePLaT we use the Pruppacher–Klett parametrization (Pruppacher and Klett, 1997):

$$r_{\text{rain}} = 0.488 P^{0.21}, \quad (7)$$

where the unit of  $r_{\text{rain}}$  is mm and the unit of rain intensity  $P$  is  $\text{mm h}^{-1}$ . Using this and other relations (Sportisse, 2007) the scavenging coefficient  $k_w$  appears in terms of rain intensity  $P$  as:

$$k_w = 0.154 P^{0.79} \text{ h}^{-1}. \quad (8)$$

For simplicity, the effect of wet deposition is taken into account only below the 850 hPa level.

These modifications due to turbulent diffusion and precipitation turn the equation of motion to a stochastic ordinary differential equation. The chaotic behavior found in this setting is thus obviously a kind of noisy chaos.

### 3 Data and Methods

As an input to the dispersion simulations, the reanalysis fields of the ERA-Interim database (Dee et al., 2011) and forecasts of the European Centre for Medium-Range Weather Forecasts (ECMWF) were used. The equations of motion of the particles are written in spherical coordinates in the horizontal, and in pressure coordinates in the vertical direction in agreement with the structure of the meteorological data used. The model solves the differential equations for the subsequent position of the particles by using the explicit Euler method. For dispersion taking place solely in the free atmosphere and for cases in which processes of the planetary boundary layer are also taken into account, the time step was chosen to be  $\Delta t = 45$  min and 5.625 min, respectively. The meteorological data are available on a given latitude-longitude grid on different pressure levels in a given time resolution. The meteorological variables at the actual location of a particle are calculated using bicubic spline interpolation in the horizontal direction and linear interpolation in the vertical direction and also in time. For particle properties we take typical volcanic ash data (Johnson et al., 2012):  $r$  in the range of 1–10  $\mu\text{m}$  and  $\rho_p = 2000$   $\text{kg}/\text{m}^3$ .

Calculation of the pollutant concentration is based on the number of particles per cells of nearly equal horizontal area. This alternative grid is constructed in the following way: the meridional sides of a “rectangular” cell is equal for all latitudes, while the zonal sides of the cells vary with latitude so that the area of the cells is almost equal, see Figure 2 (for more details see Haszpra and Tél (2013b)).

### 4 Validation: the Fukushima Accident

In order to validate the RePLaT model we simulated the dispersion of two radioactive material, the aerosol-bound cesium-137 isotope ( $^{137}\text{Cs}$ ) and the noble gas xenon-133 isotope ( $^{133}\text{Xe}$ ) released during the accident of the Fukushima Nuclear Power Plant in the spring of 2011. Wind data are taken from the ERA-Interim database. The simulations took into consideration the processes of the boundary layer, like precipitation, and turbulent diffusion depending on the height, as described in Section 2. The data of local emission were taken from the literature (Stohl et al., 2012). The dispersion of the radioactive material was followed over several weeks. The

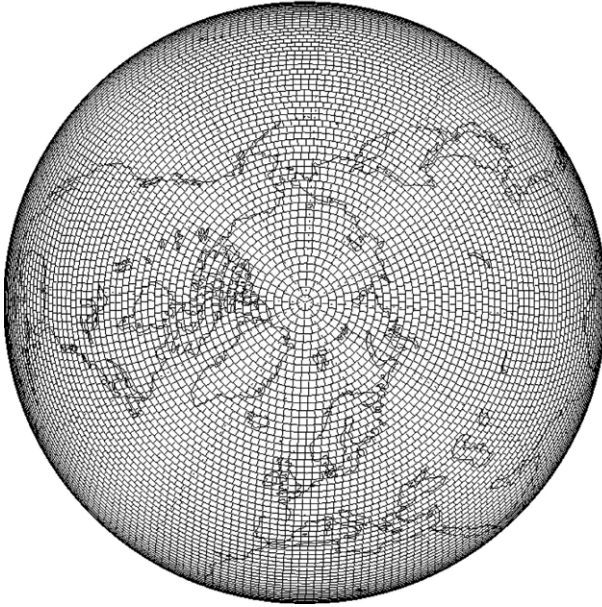


**Figure 2.** The nearly uniform-area grid used for the calculation of concentration. Here the side length of the cells is  $\varepsilon \approx 1.5^\circ$ .

radius and density of  $^{137}\text{Cs}$  carrier particles is estimated to be  $r = 0.2 \mu\text{m}$  and  $\rho_p = 1900 \text{ kg/m}^3$  based on Stohl et al. (2012), while the noble gas component was treated formally as  $r = 0$  particles (i.e. particles with zero terminal velocity) in Eq. (2). Figure 3 illustrates the geographical distribution of  $^{137}\text{Cs}$  one week after the accident. The simulation shows that the particles are transported to the East over the Pacific Ocean. In mid March a fraction of the radioactive material is captured by the steering flow of two cyclones near Japan and at the coast of North America. These particles were lifted to the free atmosphere and reached even Europe about a week later.

Figure 4 shows the access radioactivity in the first few days after its arrival to different locations. It is remarkable that the arrival times of the pollution coincide reasonable well with the measured data (dashed lines). The deviations in the intensities might be related to the fact that the emission data are estimated a posteriori via retracking methods which are subject to considerable uncertainties (Stohl et al., 2012).

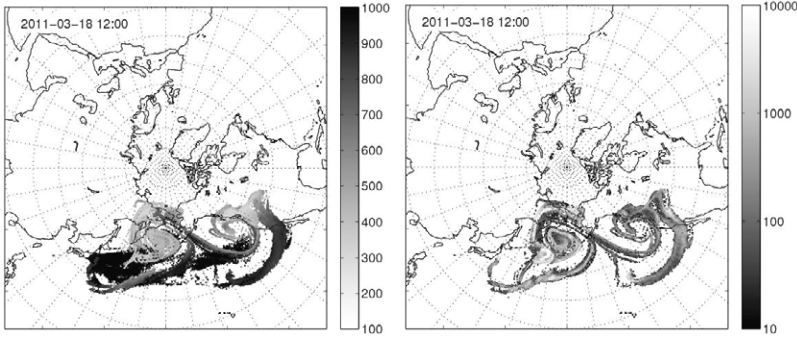


**Figure 3.** The dispersion of  $^{137}\text{Cs}$  from the Fukushima accident on March 18, 2011. Initial conditions on March 11: particles initiated in a volume of  $1^\circ \times 1^\circ$  area and height of about 300 m according to the *a posteriori* estimation of Stohl et al. (2012). Left: altitude of the carrier  $r = 0.2 \mu\text{m}$  particles in hPa. Right: radioactivity concentration in air columns over the grid of Fig. 2 originating from  $^{137}\text{Cs}$  in the unit of  $\text{Bq}/\text{m}^2$ .

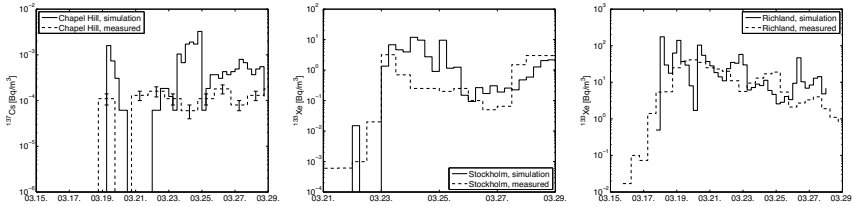


**Figure 4.** The access radioactive concentration of  $^{137}\text{Cs}$  (left) and  $^{133}\text{Xe}$  (middle and right) simulated by RePLaT (solid line) and the measured data (dashed line) as a function of the days of the year at Chapel Hill, Stockholm and Richland, respectively.

## 5 Topological Entropy

### 5.1 General Concepts

In dynamical systems theory, topological entropy is a measure of the complexity of the motion. In the most abstract setting, this quantity characterizes how the number of possible trajectories grows in time (Ott, 1993). The concept is most clearly accessible in periodically driven cases, where there exist unstable periodic orbits, so-called cycles, available for the dynamics. The temporal length of these cycles can be arbitrarily large. Moreover,

the number  $N_t$  of all the unstable cycles of length  $t$  increases drastically, exponentially for large times  $t$ . The growth rate  $h$  defined by the relation  $N_t \sim e^{ht}$  is called the topological entropy<sup>2</sup>.

The existence of  $h$  is a basic property of chaos, so much that a possible definition of chaos is based on it: a system is chaotic if its topological entropy is positive (Ott, 1993; Tél and Gruiz, 2006). The unstable cycles form the skeleton of chaos, chaotic motion can be considered as random walk among the unstable cycles. The motion might temporarily approach one of the cycles. Since, however, the cycle is unstable, the trajectory can only remain in its neighborhood for a finite time and it approaches another one sooner or later. This is the origin of the irregular nature of chaotic dynamics.

A property of topological entropy which is easier to capture in measurements is that it also represents the growth rate of the length of line segments. A line segment of initial length  $L_0$  is stretched more and more in the unstable direction of the dynamics. Let  $L(t)$  denote the length of the line segment after time  $t$ . For two-dimensional systems it is proven (Newhouse and Pignataro, 1993) that after a sufficiently long time this length increases exponentially, and the growth rate is given by just the topological entropy,  $h$ , according to the relation

$$L(t) \sim e^{ht}, \quad (9)$$

valid for  $t \gg 1/h$ . The original definition based on unstable cycles and the one relying on the growth of line segments are equivalent in time-periodic dynamics. In aperiodic problems, however, only equation (9) can be used for the definition of topological entropy, and this is the approach we follow here in the context of atmospheric dispersion.

The topological entropy  $h$  is similar in spirit to, but different in value from, the (largest positive) Lyapunov exponent  $\lambda$ . A general inequality states (Ott, 1993; Tél and Gruiz, 2006) that

$$h \geq \lambda. \quad (10)$$

The difference lies in the fact that though the Lyapunov exponent is the rate of deviation between nearby trajectories, its definition reveals that the linear growth rate of the logarithm of the distance between a particle pair should be determined. In contrast,  $h$  is the rate of change of a length (and not of its logarithm). Inequality (10) is a consequence of the mathematical

---

<sup>2</sup>The terminology is motivated by Boltzmann's relation for the thermodynamical entropy  $S$ :  $S = k_B \ln N$  known from statistical physics, where  $N$  is the number of states and  $k_B$  stands for Boltzmann's constant.

property that the logarithm of the average of a quantity is not the same as the average of the logarithm of the same quantity.

Technically, the evaluation of the topological entropy requires the monitoring of a large number of particles. This difficulty is, however, compensated by the fact that no smallness requirement or reshifting conditions are to be fulfilled (the latter are needed (Ott, 1993) for the Lyapunov calculation since the distance between the pair should always remain small). In particular, in flows represented on a grid, as in our case, the determination of the Lyapunov exponent faces the difficulty of being restricted to small scales. The determination of the topological entropy is based, however, on lengths exceeding by far the grid scale. The stretching filaments foliate regions with considerably different wind fields and are, therefore, natural candidates for providing a large scale characteristic of the atmosphere. Altogether, our experience shows that the numerical determination of the topological entropy appears to be straightforward and computationally rather cheap.

## 5.2 A Case Study

In the atmospheric context, the use of topological entropy is based on the general observation that any initially short material line becomes strongly stretched within a short time. We illustrate the usefulness of the concept with a case study within the RePLaT model. Wind data are taken from the ERA-Interim database again. For simplicity, first we consider ideal tracers ( $r = 0$ ) within the free atmosphere where turbulent diffusion is negligible ( $\mathbf{D} = 0$  in (4)), and no precipitation takes place ( $P = 0$ ).

Fig. 5 illustrates the dispersion of an initially meridional line segment of  $n = 2 \cdot 10^5$  particles with an initial length  $L_0 = 3^\circ \approx 333$  km (twice the resolution of the wind data) initialized between Great Britain and Scandinavia and followed for a period of 10 days. In the first days the particles are advected to Northeast towards the Scandinavian Peninsula, while the length of the filament increases. On the fourth day (Figure 5 left) the middle part of the filament is captured by a cyclone over Finland, while the easterly end also begins to spiral around another cyclone over Siberia. During the next few days (Figure 5 middle and right) the cyclones and anticyclones of the atmospheric flow fold, rumple and lengthen the filament more and more by stirring, and at the end of the observation period of 10 days the extent of the line segment becomes 6–7000 times longer than the initial length (Figure 6), and extends over Europe and quite a large area of Asia. It is also interesting, as can be read off from the grayscale of the right panel of Figure 5, that after 10 days the altitude of the particles spans to a range between about 300–1000 hPa, corresponding to about 9 km in altitude.

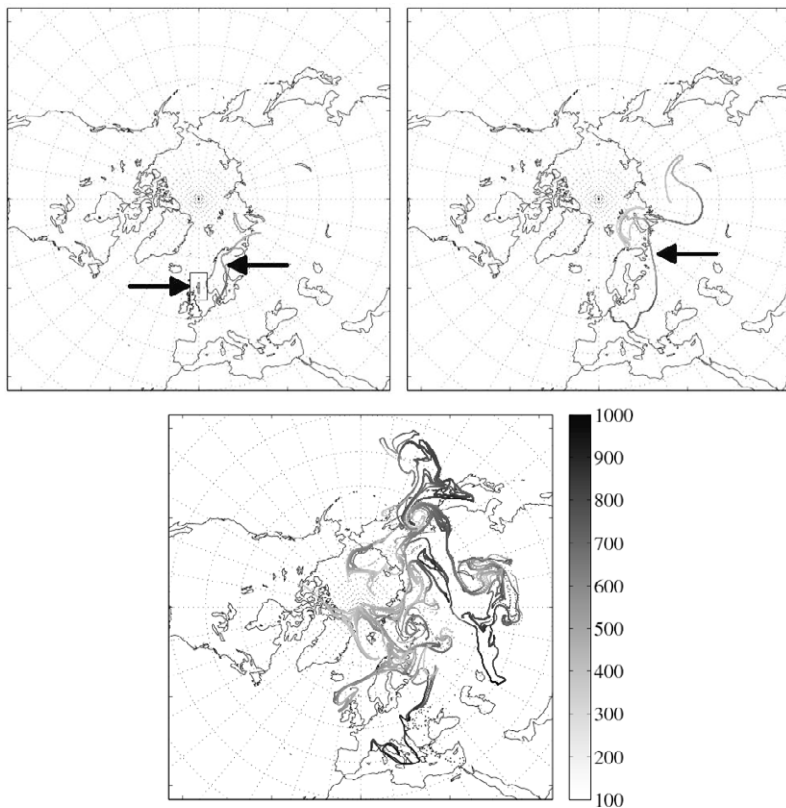


**Figure 5.** Stretching of a material line initialized at 00 UTC June 1, 2010. Initial conditions (surrounded by a box):  $L_0 = 3^\circ \approx 333$  km,  $n_0 = 2 \times 10^5$  particles were distributed along a meridian on  $p_0 = 500$  hPa, the center of the line was  $\lambda_0 = 0^\circ$ ,  $\varphi = 60^\circ$ N. The panels show the location of the particles after 4, 6 and 10 days after the release, respectively. The arrows in the upper panels point toward the pollutant cloud. The altitude of the particles in pressure coordinates is marked by grayscale.

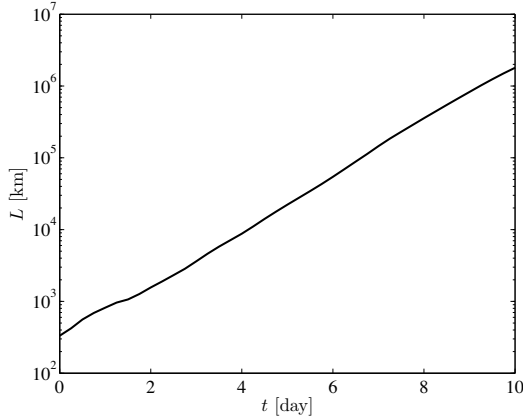


**Figure 6.** The length  $L(t)$  of the material line shown in Figure 5 as a function of time over 10 days.

The length  $L(t)$  of the filament at time  $t$  is computed as the sum of the horizontal distances between neighboring particle positions. It is clearly visible in Fig. 6 that the growth of  $L(t)$  is exponential in time. The exponent, the topological entropy is found to be  $h = 0.89 \text{ day}^{-1}$ . This implies that the total stretching factor after 10 days is  $\exp(8.9) \approx 7330$ , in harmony with the estimate above.

### 5.3 Geographical Distribution of Topological Entropy

One can observe quite remarkable differences in the topological entropy values depending on the initial geographical location and also on the particular season. To gain a systematic understanding, we extended our studies to small (up to  $r = 5 \mu\text{m}$ ) aerosol particles and to different locations (Haszpra and Tél, 2011). We initialized material line segments oriented meridionally over the Globe, distributed on a grid: from  $80^\circ\text{S}$  to  $80^\circ\text{N}$  in  $10^\circ$  increments, and from  $180^\circ\text{W}$  to  $180^\circ\text{E}$  in  $30^\circ$  increments. The initial height is  $p_0 = 500 \text{ hPa}$ . The topological entropy of each line segment is calculated from a 10-days tracking. The results for  $r = 1 \mu\text{m}$  particles obtained on the 1st of January 2010 are shown in Figure 7. The largest topological entropies ( $\approx 0.7 \text{ day}^{-1}$ ) appear in the midlatitudes, and can be attributed to the strong mixing and shearing effects of the cyclones. The smallest values ( $\approx 0.2 \text{ day}^{-1}$ ) can be found in the tropical belt.

The zonal average of these topological entropy values is of double-hill

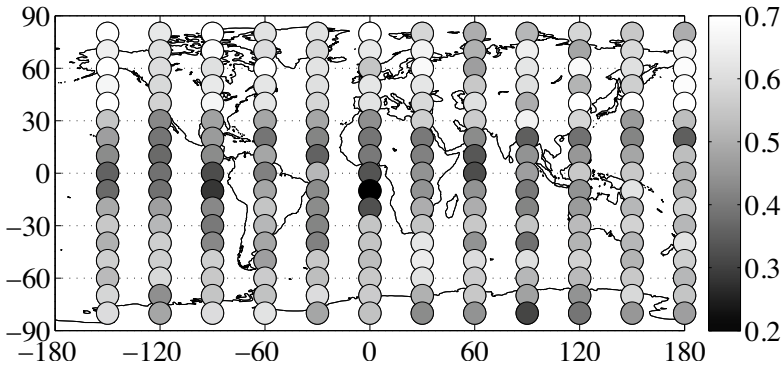


**Figure 7.** Geographical distribution of the 10-day-topological entropy of material lines of  $r = 1 \mu\text{m}$  particles. The material lines were distributed on the 500 hPa level on 01.01.2010 00 UTC in the center of the circles shown, their initial length was  $L_0 \approx 333 \text{ km}$ .

shape (see Fig. 8), with somewhat larger values in the winter than in the summer hemisphere.

#### 5.4 Remarks

We also carried out (Haszpra and Tél, 2013b) an investigation of the seasonal change of the topological entropy. To this end, at each geographical location, a line segment is initialized in every 10 days, then the temporal average of the topological entropy of three months is determined for December to February, March to May, June to August, and September to November. The largest values appear in the mid and high latitudes, mainly in the winter season of the hemisphere due to the strong mixing and shearing effects of cyclones. The zonally averaged topological entropy in the mid- and high latitudes ( $30^\circ\text{--}80^\circ$ ) in the winter season of both hemispheres is somewhat larger than in the summer ( $\bar{h}_w - \bar{h}_s \approx 0.06 \text{ day}^{-1}$ ). This is in agreement with the fact that winters are more variable than summers because of the greater temperature gradient between the pole and the Equator (see also Figure 8). The difference between the winter and summer season is more significant on the Southern Hemisphere than on the Northern one ( $0.09$  and  $0.04 \text{ day}^{-1}$ , respectively). The reason for this can be the difference in the proportion and location of oceans and continents. The average topological entropy was found to depend only slightly on the initial altitude of the particles.

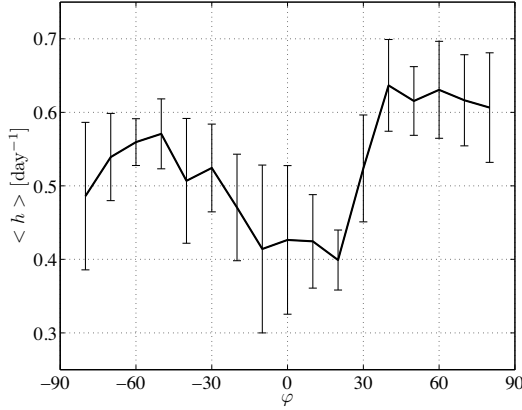


**Figure 8.** The zonal average of the topological entropy of Figure 7. The error bar denotes the standard deviation of the topological entropy values along a latitude.

It is worth noting that the atmosphere as a single system should be characterizable by a single value of the topological entropy. This is indeed valid for long term (of several months) observations. The 10-day-topological entropy used here is in fact a new location-dependent quantity, and it is a surprising empirical fact that a well-defined exponential scaling can be observed during such a short time. Anyhow, this local value of the topological entropy can be considered to be a new, useful measure of the chaoticity of the state of the atmosphere, and it can provide information on the speed of pollutant spread from a given location.

## 6 Escape Rate

### 6.1 General Concepts

Under certain circumstances chaotic behavior is of finite duration, i.e., the complexity and unpredictability of the motion can be observed over a *finite time interval* only. Nevertheless, there also exists in such cases a set in phase space responsible for chaos, which is, however, non-attracting. This type of chaos is called *transient chaos* and the non-attracting set is a *chaotic saddle* (for an introductory text see Tél and Gruiz, 2006). Since there are typically significant differences in the individual lifetimes, an *average* lifetime can be defined. To this end, it is worth following several motions instead of a single one: the study of particle ensembles is essential. To

characterize the dynamics, one takes a preselected region, and starts  $n_0 \gg 1$  trajectories in it. They escape the preselected region sooner or later, and the motion before escape appears to be chaotic. The number  $n(t)$  of trajectories that do not leave the preselected region up to time  $t$  is thus a monotonically decreasing function of  $t$ . After a sufficiently long time (for  $t$  larger than some  $t_c$ ), the decay in the number  $n(t)$  of survivors is generally exponential:

$$n(t) \sim \exp(-\kappa t), \quad \text{for } t > t_c. \quad (11)$$

Coefficient  $\kappa$  is called the *escape rate* (Ott, 1993; Tél and Gruiz, 2006; Lai and Tél, 2011). Its reciprocal value can be considered as an estimate of the average lifetime of chaos. A nonzero escape rate is thus a new, important chaos characteristic: the larger the value of  $\kappa$ , the faster the escape/sedimentation process.

In the atmospheric context, the preselected region might be the entire atmosphere. The condition of escape is then the first arrival at the surface. It is interesting to see how turbulence and wet deposition influence the escape dynamics. We claim that the escape rates provide a kind of Lagrangian characterization of the entire deposition process.

## 6.2 Global Results

In order to determine global escape rates, we distribute  $n_0 = 2.5 \times 10^5$  particles uniformly over the globe on different pressure levels on 1 January 2010. They are tracked in the ERA-Interim wind fields up to their escape, but at longest for 1 yr. To study the dependence of the escape rate on the particle size and on the initial altitude, simulations are run with radii of  $r = 0, 1, 2, \dots, 12 \mu\text{m}$  and initial altitudes of  $p_0 = 500, 700, 850$  and  $900 \text{ hPa}$  (Haszpra and Tél, 2013a). Note that the radius of a particle suddenly changes if the particle is captured by a raindrop, as discussed in the description of the RePLaT model (Section 2). (The limiting case of a “particle” with  $r = 0 \mu\text{m}$  can be considered as a gaseous contaminant in the atmosphere.)

To compare different effects, simulations are carried out in three setups that take into account:

1. advection, turbulent diffusion and precipitation,
2. advection and turbulent diffusion, and
3. only advection.

As a first example, Fig. 9 exhibits the number of survivors vs. time for a fixed initial altitude  $p_0 = 500 \text{ hPa}$  (corresponding to free atmospheric initial conditions) for  $r = 9 \mu\text{m}$  particles in setup 1. As the aerosol particles are initially far from the surface, the curve starts with a plateau: no

outfall from the atmosphere occurs within the first few days. After a short transition following the plateau (i.e. for  $t > t_c \approx 1\text{--}15$  days for the different simulations), an approximately exponential decay can be seen for a few days (see the dashed line belonging to days 2–5 in Fig. 9). After some time, however, a crossover takes place and a slower exponential decay sets in for  $t > 10$  days). Thus, we can speak of a short-term and a long-term exponential decay characterized by different exponents. The corresponding escape rates will be denoted by  $\kappa_s$  and  $\kappa_\ell$ , respectively.

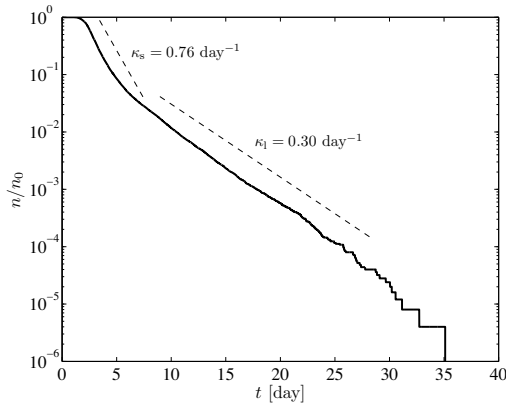


**Figure 9.** Proportion  $n/n_0$  of the number of survivors in setup 1 as a function of time.  $n_0 = 2.5 \times 10^5$  particles were distributed uniformly over the globe on  $p_0 = 500$  hPa with  $r = 9 \mu\text{m}$  on 01.01.2010 00 UTC. Dashed lines illustrate the short-term and long-term decay processes.

Escape rates can be used as measures of the deposition process. Results obtained for different sizes show that both escape rates are at least 10 times larger for large aerosol particles (9 or 10  $\mu\text{m}$ ) than for small ones. The deposition process is thus very fast for large sizes. At any given size, the long-term escape rate is at least half or smaller than the short-term one. Since this difference appears in the exponent, we can safely speak about a separation of time scales in the deposition process.

Our findings illustrate that the naive expectation coming from dynamical systems theory according to which the global emptying is a random process described by a single exponential decay does not hold. In the atmosphere, instead, a short-term and a long-term dynamics can be identified, characterized by two different approximately exponential decays.

A detailed investigation shows that the long-term escape rate  $\kappa_\ell$  com-

puted for different initial pressure levels  $p_0$  does *not* depend on the initial level in either setup (in contrast to  $\kappa_s$  which exhibits a strong  $p_0$ -dependence). The reason for this phenomenon might be the fact that particles surviving a long time in the atmosphere become well mixed. The independence of  $p_0$  indicates that there exists a *global atmospheric chaotic saddle*, and the long-lived particles reflect properties of this set underlying the deposition dynamics.  $\kappa_\ell(r)$  is thus a global atmospheric characteristic of particles of size  $r$ . The atmospheric saddle is likely to be time-dependent, and the  $\kappa_\ell(r)$  values are characteristic of the time period investigated.

It is remarkable that  $\kappa_\ell$  ranges over about two orders of magnitude although the radii vary over one decade only. The dependence is thus strongly nonlinear. The best approximate fit appears to be exponential

$$\kappa_\ell(r) \sim \exp(kr). \quad (12)$$

Exponent  $k$  is found to be  $k \approx 0.33\text{--}0.38 \mu\text{m}^{-1}$  for setups 1, 2, including rain and/or turbulent diffusion (see Fig. 10).

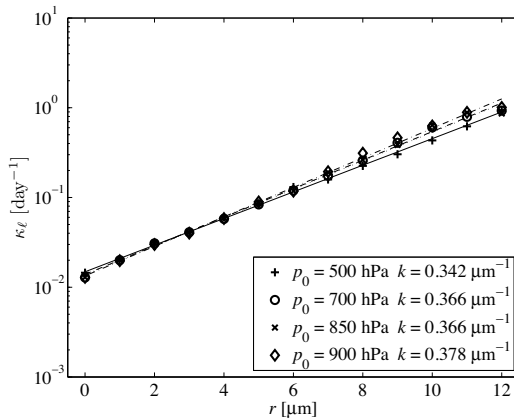


**Figure 10.** The dependence of the long-term escape rate on the size and initial altitude of the particles in setup 2 for different  $p_0$  levels. Dashed lines indicate exponential fittings to  $\kappa_\ell$  vs.  $r$ .

It is worth comparing the scaling of Eq. (12) with a naive estimate. The time needed to pass a fixed vertical distance  $Z$  with the terminal velocity (3) in non-moving air is  $Z/w_{term}$ . Since the terminal velocity is proportional to  $r^2$ , the time is proportional to  $r^{-2}$ . As the reciprocal of this time corresponds to the escape rate, the estimate results in a scaling proportional to  $r^2$ . The fit of this functional form to the data is much less satisfactory

than that provided by (12). The difference between the power law behavior and the observed exponential one can only be interpreted by realizing that atmospheric winds play an essential role in the deposition process.

### 6.3 The Eruption of Mount Merapi

Mount Merapi in Indonesia had long-lasting eruption series in 2010, from late October to November. To study the outfall dynamics of aerosol particles, instead of the continuous eruptions, we simulate with RePLaT only a single volcanic ash puff of columnar shape of size  $1^\circ \times 1^\circ \times 400$  hPa, centered at  $\lambda_0 = 110.44^\circ$  E,  $\varphi_0 = 7.54^\circ$  S and  $p_0 = 500$  hPa (Haszpra and Tél, 2013a).

Figure 11 demonstrates the horizontal dispersion of the ash cloud containing  $n_0 = 2.16 \times 10^5$  particles of  $r = 5 \mu\text{m}$  emitted at 00 UTC on 1 November in the ERA-interim wind field. As expected, such particles spread and reach very different regions in the atmosphere. Entering into different vertical levels, they become subject to different horizontal winds. The still strongly localized ash cloud on the 3rd day (Fig. 11, top left) spreads considerably up to the 7th day (Fig. 11, top right). It is worth mentioning that despite the simplifying one-puff assumption, this figure shows good agreement with the satellite image of sulfur dioxide tracers in the period of 4–8 November (<http://earthobservatory.nasa.gov/NaturalHazards/view.php?id=46881>). 20 days after the hypothetical emission, the particles initialized in a small volume cover a huge area and are well mixed in the midlatitudes of the Southern Hemisphere. Therefore the long-term escape rate found for this case ( $\kappa' = 0.103 \mu\text{m}^{-1}$ ) is almost the same as the global escape rate  $\kappa_\ell$  for  $r = 5 \mu\text{m}$  particles.

A remarkable feature of the bottom panel of Fig. 11, showing the ash cloud 20 days after the eruption, is that the distribution of the deposited (black) particles is fractal-like. There are large regions without any outfall, and the overall pattern is filamentary. The set of particles on the surface appears to trace out the intersection of the unstable manifold of the atmospheric chaotic saddle with the surface. This saddle might in principle be time-dependent, and what we see here is the set of these intersections in the interval November 7–20.

It is insightful to look at the vertical distribution of the particles over the time span followed. This can be seen in the form of a histogram in Fig. 12 for particles of  $r = 10 \mu\text{m}$ . The initially columnar shape is deformed into a Gaussian one that spreads as its center moves downwards. This behavior was also observed in a simple cloud model with aerosol particles (Drótos and Tél, 2011). It is remarkable, however, that after the center of the

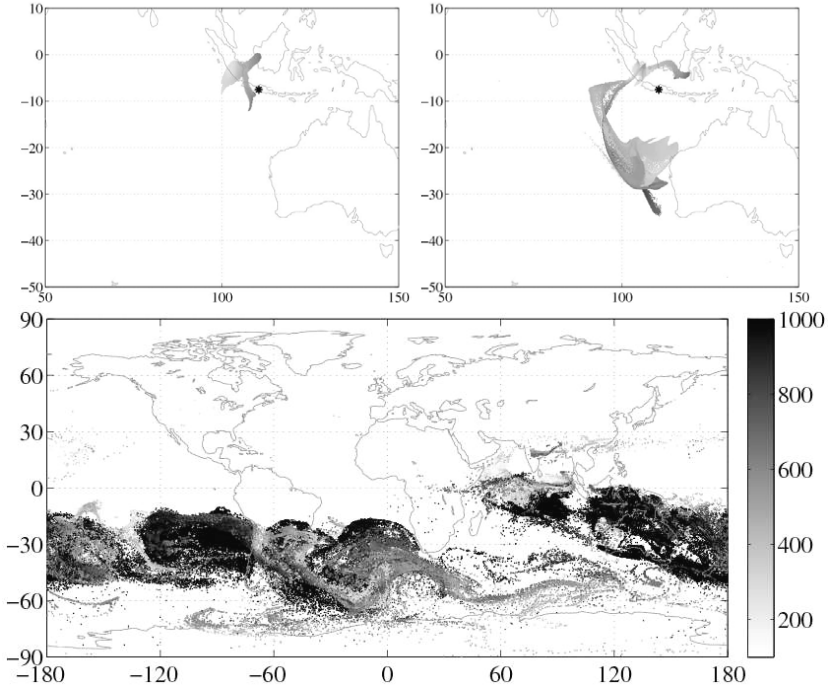


**Figure 11.** Dispersion of the volcanic ash consisting of  $r = 5 \mu\text{m}$  particles from the Mount Merapi eruption. Panels illustrate the geographical distribution 3, 7 and 20 days after the eruption taken place on 1 November, 2010, respectively. Graybar indicates the pressure level of the particles in hPa.

Gaussian distribution reaches the surface, and the majority of the particles is deposited, the small fraction of particles remaining aloft is distributed *widely* in the different layers. It is the fraction of these extreme survivors that is responsible for the second, long-term exponential decay observed. We believe that this wide altitudinal distribution of the extreme survivors is also the physical background of the time-scale separation described in the previous section.

#### 6.4 Remarks

It is interesting to compare the escape process with precipitation activities. Only a small fraction of the  $r = 10 \mu\text{m}$  particles is found to leave the atmosphere in the first 6 days after the hypothetical eruption of Mount

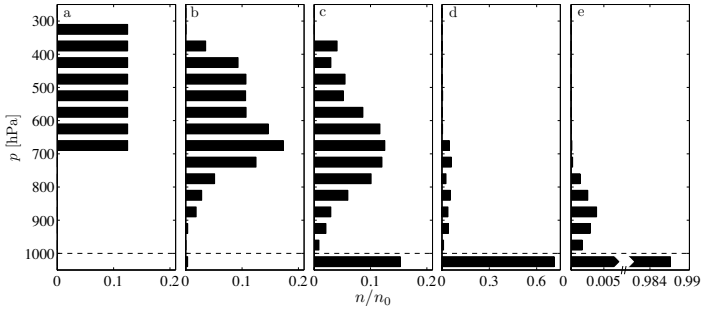


**Figure 12.** Vertical distribution of the proportion of particles with  $r = 10 \mu\text{m}$  in vertical layers of size 50 hPa for 0, 1, 3, 5, and 7 days after the hypothetical Mount Merapi eruption. The dashed horizontal line represents the surface.

Merapi. When they happen to reach the 850 hPa level precipitation starts playing an important role due to the frequent rainfall events above Indonesia. In the period of days 6–8 (6–8 November), particles reach a region of a cyclone with strong precipitation, therefore a large amount of particles are scavenged out by rain in this period. The particle distribution on the surface is found to strongly correlate with the rain intensity (Haszpra and Tél, 2013a). Indeed within 8 days, the majority of the particles falls out from the atmosphere in this case.

In summary, we have found that the emptying process of aerosol particles cannot be characterized by a single exponential decay. The global emptying process, from any height of the atmosphere, is governed by two temporal periods in which different exponential forms appear defining two different escape rates. The reciprocal value of the short-term escape rate is found to provide an estimate of the average residence time of typical particles. The analogous quantity belonging to the long-term escape rate characterizes exceptional particles that remain in the atmosphere for an extremely long time. It is interesting to note that the escape rates of particles of different sizes are found to vary in a broad range rather rapidly, roughly exponentially with the particle size. These investigations provide a Lagrangian foundation for the concept of deposition rates.

## 7 Ensemble Features and Outlook

It is important to note that there is always some uncertainty in the calculation of pollutant dispersion due to different error sources. One of these is

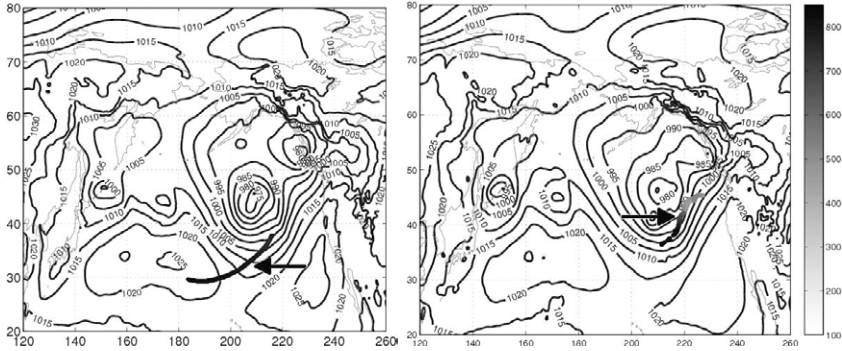
the meteorological forecast produced by the numerical solution of the partial differential equations of the atmospheric hydrodynamics. Due to inaccuracies in the measurements and approximations used, the initial conditions of the meteorological model cannot be determined precisely. Initial errors are then amplified because of the sensitivity to initial conditions of atmospheric turbulence. Therefore, there is uncertainty in the meteorological forecasts which can be quantified by the so-called ensemble technique based on the execution of multiple meteorological simulations (Kalnay, 2003; Leutbecher and Palmer, 2008). These imply that there is a considerable difference in the driving provided by the velocity field  $\mathbf{v}$  for the advection equations (2) or (4).

Dispersion models are usually run by a single forecast which is considered to be the best one. However, it can be useful to perform simulations using the whole ensemble forecast, i.e. producing an ensemble dispersion prediction in order to get a detailed and more reliable overview of the uncertainties and possible hazards related to the dispersion event.

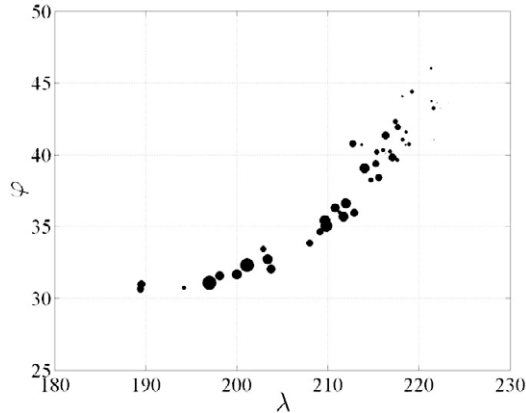
Figure 13 shows the distribution of  $r = 1 \mu\text{m}$  particles in two ensemble members of an ECMWF ensemble forecast after 2.5 days tracking with the RePLaT model. The particles are initiated in a two-dimensional square of size  $1^\circ \times 1^\circ$ , centered at  $\lambda = 141^\circ\text{E}$ ,  $\varphi = 37.5^\circ\text{N}$  and  $p_0 = 500 \text{ hPa}$  at 00 UTC 12 March, 2011 (as a hypothetical emission well above the original emission height of the Fukushima Power Plant accident). For simplicity, we study only the effect of the variability in the wind field and do not take into account the impact of turbulent diffusion and precipitation (Haszpra et al., 2013; Haszpra and Horányi, 2014). Figure 13 demonstrates that even with this restriction strong dispersion variabilities may develop between the members both in the horizontal/vertical location and in the extension of the pollutant cloud in spite of the rather short time (2.5 days) passed after the emission.

Figure 14 provides a more systematic illustration of this statement. One can see that the horizontal locations of the center of mass of the pollutant clouds in the different ensemble members extend to a quite large area. The largest distance between the centers of mass is about 3375 km, on the order of half of the radius of the Earth. Also the standard deviations of the particles in the clouds, represented by the radii of the circles, vary in a wide range (from 35 km to 960 km). All this suggests that the problem of pollutant spreading should also be treated in the spirit of ensemble forecasts. The ensemble variability turns out to be rather strong and appropriate statistical measures should be introduced, some of which have been worked out in Haszpra et al. (2013).

In this paper we argued that a proper treatment of atmospheric material



**Figure 13.** Geographical distribution of the pollutant cloud of  $r = 1 \mu\text{m}$  particles obtained from the 11th and 19th member of the ensemble forecast of ECMWF with RePLaT 2.5 days after the release at 00 UTC March 12, 2011 shown in the left and right panel, respectively. Graybar indicates the altitude of the particles in hPa. Contour lines represent the mean sea level pressure. The horizontal length of the pollutant cloud is about 2 times larger in the left than in the right panel, whereas the relation of the vertical extensions is approximately the opposite with a factor of about 3. The centers of mass are about 2000 km away from each other. The arrows point toward the pollutant clouds.



**Figure 14.** The horizontal geographical location of the center of mass of the pollutant clouds of  $r = 1 \mu\text{m}$  particles in the atmosphere for the 51 ensemble members after 2.5 days. The radii of the circles are proportional to the standard deviation of the clouds.

dispersion should be based on individual particle tracking using realistic size and density. The effect of turbulent diffusion and the scavenging of particles by precipitation can be incorporated as stochastic perturbations. This approach enables one to investigate the chaotic aspects of particle dispersion by means of dynamical systems concepts. The topological entropy and the escape rate were shown to be two useful measures not applied earlier in the atmospheric context. The uncertainty in the dispersion due to the unpredictability of the meteorological forecasts can also be studied.

All these features are, of course, subject to changes in the climatic conditions. For example, more intense local atmospheric circulation with more frequent and/or stronger cyclones might induce more stretched material lines generally and, along with this, larger 10-day-topological entropy values. In spite of these features, the global 10-day- and long-term topological entropies might become smaller than the corresponding values today due to the predicted (IPCC, 2013) decrease of the meridional temperature gradients in the future. The occurrence of high precipitation events might increase the proportion of the outfalling particles locally, while regions with less precipitation and possibly stronger updrafts than during present climate conditions can decrease the deposition. The overall effect to the value of the escape rate would require additional numerical simulations. More intense local circulation might also enhance the uncertainty of meteorological forecasts and, therefore, it might increase the variability of the ensemble dispersion simulations based on these forecasts. The detailed investigation of these issues remains a task for the future.

## Acknowledgements

The authors would like to thank G. Drótos, Z. Ferenczi, V. Homonnai, A. Horányi, I. Ihász, L. Lagzi and G. Wotawa for useful comments and remarks. This work was supported by the Hungarian Science Foundation under Grant no. OTKA NK100296 and by the von Humboldt Foundation.

## Bibliography

- H. Aref. Stirring by chaotic advection. *Journal of Fluid Mechanics*, 143(1): 1–21, 1984.
- D. P. Dee et al. The ERA-Interim reanalysis: Configuration and performance of the data assimilation system. *Quarterly Journal of the Royal Meteorological Society*, 137(656):553–597, 2011.
- R. R. Draxler and G. D. Hess. *Description of the HYSPLIT\_4 modeling system*. Air Resources Laboratory, Silver Spring, Maryland, 2004. NOAA

- Technical Memorandum ERL ARL-224.
- G. Drótos and T. Tél. Chaotic saddles in a gravitational field: The case of inertial particles in finite domains. *Physical Review E*, 83(5):056203, 2011.
- A. J. Dyer. A review of flux-profile relationships. *Boundary-Layer Meteorology*, 7:363–372, 1974.
- T. Haszpra and A. Horányi. Some aspects of the impact of meteorological forecast uncertainties on environmental dispersion prediction. *Időjárás*, 118(4):335–347, 2014.
- T. Haszpra and T. Tél. Volcanic ash in the free atmosphere: A dynamical systems approach. *Journal of Physics: Conference Series*, 333:012008, 2011.
- T. Haszpra and T. Tél. Escape rate: a Lagrangian measure of particle deposition from the atmosphere. *Nonlinear Processes in Geophysics*, 20(5):867–881, 2013a. doi: 10.5194/npg-20-867-2013.
- T. Haszpra and T. Tél. Topological entropy: a Lagrangian measure of the state of the free atmosphere. *Journal of the Atmospheric Sciences*, 70(12):4030–4040, 2013b. doi: 10.1175/JAS-D-13-069.1.
- T. Haszpra, I. Lagzi, and T. Tél. Dispersion of aerosol particles in the free atmosphere using ensemble forecasts. *Nonlinear Processes in Geophysics*, 20(5):759–770, 2013. doi: 10.5194/npg-20-759-2013.
- J. L. Heffter and B. J. B. Stunder. Volcanic Ash Forecast Transport And Dispersion (VAFTAD) model. *Weather and Forecasting*, 8(4):533–541, 1993.
- IPCC(2013). *Climate Change 2013: The Physical Science Basis, Working Group I Contribution to the Fifth Assessment Report of the Intergovernmental Panel on Climate Change*. Cambridge University Press, New York, 2013.
- B. Johnson et al. In situ observations of volcanic ash clouds from the faam aircraft during the eruption of eyjafjallajkull in 2010. *Journal of Geophysical Research: Atmospheres*, 117(D20), 2012. ISSN 2156-2202. doi: 10.1029/2011JD016760.
- E. Kalnay. *Atmospheric modeling, data assimilation and predictability*. Cambridge University Press, Cambridge, 2003. ISBN 0-521-79179-0.
- Y.-C. Lai and T. Tél. *Transient Chaos: Complex Dynamics on Finite Time Scales*. Springer, New York, 2011. ISBN 978-1-4419-6986-6.
- M. Leutbecher and T. N. Palmer. Ensemble forecasting. *Journal of Computational Physics*, 227:3515–3539, 2008.
- S. Newhouse and T. Pignataro. On the estimation of topological entropy. *Journal of Statistical Physics*, 72:1331–1351, 1993.
- E. Ott. *Chaos in Dynamical Systems*. Cambridge, 1993.

- 
- H. R. Pruppacher and J. D. Klett. *Microphysics of Clouds and Precipitation*. Kluwer Academic Publishers, Dordrecht, Netherlands, 1997. ISBN 978-0-7923-4211-9.
- C. Searcy, K. Dean, and W. Stinger. PUFF: A high-resolution volcanic ash tracking model. *Journal of Volcanology and Geothermal Research*, 80: 1–16, 1998.
- J. H. Seinfeld and S. N. Pandis. *Atmospheric Chemistry and Physics: From Air Pollution to Climate Change*. John Wiley & Sons, Inc., 1998. ISBN 0-471-17815-2.
- B. Sportisse. A review of parameterizations for modelling dry deposition and scavenging of radionuclides. *Atmospheric Environment*, 41(13):2683–2698, 2007.
- A. Stohl et al. *The Lagrangian particle dispersion model FLEXPART version 8.2*, 2010. Technical report.
- A. Stohl et al. Xenon-133 and caesium-137 releases into the atmosphere from the Fukushima Dai-ichi nuclear power plant: determination of the source term, atmospheric dispersion, and deposition. *Atmospheric Chemistry and Physics*, 12(5):2313–2343, 2012.
- T. Tél and M. Gruiz. *Chaotic Dynamics: An Introduction Based on Classical Mechanics*. Cambridge University Press, 2006. ISBN 978-0-512-83912-9.
- I. B. Troen and L. Mahrt. A simple model of the atmospheric boundary layer; sensitivity to surface evaporation. *Boundary-Layer Meteorology*, 37:129–148, 1986.